Competing magnetic and nonmagnetic states in monolayer VSe_2 with charge density wave

Li Yin [1,*] Tom Berlijn [2] Rinkle Juneja [1] Lucas Lindsay [1] and David S. Parker [1]

[1]*Material Science and Technology Division, Oak Ridge National Laboratory, Oak Ridge, Tennessee 37831, USA*

[2]*Center for Nanophase Materials Sciences, Oak Ridge National Laboratory, Oak Ridge, Tennessee 37831, USA*

(Received 25 March 2022; revised 21 June 2022; accepted 26 July 2022; published 11 August 2022)

The field of two-dimensional ferromagnets has been reinvigorated by the discovery of VSe_2 monolayer grown on van der Waals substrates, which is reported to be ferromagnetic with a Curie point higher than 330 K. However, the ferromagnetic and nonmagnetic states of pristine monolayer VSe_2 are highly debated. Here, employing density functional theory, Wannier function calculations, and the band unfolding method, we explore the electronic structure of monolayer VSe_2 with a $\sqrt{3} \times \sqrt{7}$ charge density wave (CDW). Certain qualitative aspects of the calculated unfolded band dispersion and unfolded Fermi surface of monolayer VSe_2 with the $\sqrt{3} \times \sqrt{7}$ CDW in the nonmagnetic state agree well with previous angle-resolved photoemission spectroscopy results, albeit with uncertainty about whether these experiments probed single or multiple domains. Specifically, we find that an isolated CDW domain naturally induces a strong breaking of the threefold symmetry of the electronic structure. In addition we find that, relative to the undistorted structure, the CDW structure shows a strong competition between nonmagnetic and various magnetic states, with an energy difference less than 5 meV/f.u. For the CDW structure in the antiferromagnetic state, the band dispersions and Fermi surface are similar to those in the nonmagnetic state, while the unfolded bands of the ferromagnetic CDW state display a sizable exchange splitting. These results indicate the possibility of various antiferromagnetic fluctuations in VSe_2 to coexist and compete with ferromagnetic order and the experimentally reported CDW order. Our calculations build insights for exploring the interplay between magnetism and CDW behaviors more generally in transition metal dichalcogenides.

DOI: 10.1103/PhysRevB.106.085117

I. INTRODUCTION

Owing to rapidly developing theoretical and fabrication methods [1–3], two-dimensional (2D) crystals [4,5] with diverse functionalities have been synthesized, characterized, and utilized, including metals, semimetals, semiconductors, topological insulators, topological superconductors [6,7], and systems with long-range electric [8] and magnetic orders [5]. In particular, the families of 2D magnets have been developing rapidly since intrinsic ferromagnetism was revealed in CrI_3 and Cr_2Ge_2Te [9,10]. Long-range magnetic order in 2D materials is typically weaker than that in the 3D case, but stronger than that in the 1D case [4]. As an intermediate case, the long-range magnetic order in 2D systems is highly dependent on the magnetic anisotropy, which is also described by the so-called spin dimensionality. The spin dimensionality of $n = 1$, 2, and 3 denote the uniaxial magnetic anisotropy, planar magnetic anisotropy, and magnetic isotropy respectively, which can be described by the localized Ising-Lenz ($n = 1$, such as the above mentioned CrI_3) [11,12], XY ($n = 2$) [13,14], and Heisenberg ($n = 3$, such as the above mentioned Cr_2Ge_2Te) [15] models.

So far, various magnetic 2D materials distinguished by the magnetic intralayer and interlayer structure have been found [4], such as the ferromagnetic Cr_2Ge_2Te and CrI_3, with either intralayer antiferromagnetism or ferromagnetism, depending on the number of layers, the interlayer antiferromagnetic $MnPS_3$, and the intralayer and interlayer antiferromagnetic $FePS_3$ [4,5]. Among these 2D magnets, ferromagnetism only occurs in few materials: CrI_3, Cr_2Ge_2Te, Fe_3GeTe_2, and VSe_2. The Curie temperature is less than 70 K in CrI_3 or Cr_2Ge_2Te [9,10] and within 140–220 K in Fe_3GeTe_2 [5,16,17], which is not ideal for applications. However, VSe_2 monolayers grown on van der Waals substrates are reported to be ferromagnetic with a Curie temperature larger than 330 K [18]. Although some studies report that the molecular-beam-epitaxy-grown VSe_2 monolayer lacks intrinsic ferromagnetism [19–21], the prospect of room-temperature ferromagnetism in monolayer VSe_2 remains appealing.

Based on a series of experimental studies, a consensus is emerging that the intrinsic ferromagnetism of the monolayer VSe_2 is suppressed by charge density waves (CDWs) [19,22,23]. To date, different kinds of CDWs have been found in monolayer VSe_2, including the $\sqrt{3} \times \sqrt{7}$ CDW [18,19], the 4×4 CDW [20], and the mixed $2 \times \sqrt{3} - \sqrt{3} \times \sqrt{7}$ CDW [24–26]. In particular, the CDW-induced gap in monolayer VSe_2 varies substantially, with values ranging from 100 meV in the $\sqrt{3} \times \sqrt{7}$ CDW to 26 meV in the mixed $2 \times \sqrt{3} - \sqrt{3} \times \sqrt{7}$ CDW. Even among CDWs with the same $\sqrt{3} \times \sqrt{7}$ periodicity, the measured gap varies from 100 meV [19] to 55 meV [18]. These results highlight that CDWs, especially the $\sqrt{3} \times \sqrt{7}$ CDW with pronounced imaginary

*Corresponding author: yinl@ornl.gov

modes in the phonon dispersion of undistorted monolayer VSe_2 at the q point that correspond to a commensurate $\sqrt{3} \times \sqrt{7}$ distortion [19], play an important role in monolayer VSe_2. However, in former theoretical calculations [27,28], the magnetism and the ferromagnetic ground state in monolayer VSe_2 were demonstrated in the perfect lattice structure, in the absence of a CDW. Meanwhile, angular resolved photoemission spectroscopy (ARPES) experiments [19,20] indicate no detectable ferromagnetic exchange band splitting in monolayer VSe_2. In addition, evidence for magnetic frustration in monolayer VSe_2 has been reported [26]. Overall, the magnetic structure of monolayer VSe_2 is rather ambiguous.

A further complication resides in the nonstoichiometry of monolayer VSe_2. Room-temperature ferromagnetism has been confirmed in chemically exfoliated VSe_2 monolayers with Se vacancies [29]. VSe_2 monolayers reconstructed by Se-deficient line defects are also demonstrated to be ferromagnetic above room temperature [30]. The formation of the mixed $2 \times \sqrt{3}$ $-\sqrt{3} \times \sqrt{7}$ CDW is also mostly attributed to the distortion of Se atoms, rather than the reordering of charges on the V atoms [25]. These results show the importance of Se atoms for the structure and magnetic order of monolayer VSe_2.

In this work, employing density functional theory, Wannier function calculations, and the band unfolding method, we study the electronic structure of monolayer VSe_2 with a $\sqrt{3} \times \sqrt{7}$ CDW. Certain qualitative aspects of the calculated unfolded band dispersion and unfolded Fermi surface of monolayer VSe_2 with the $\sqrt{3} \times \sqrt{7}$ CDW in the nonmagnetic state agree well with previous ARPES results, up to an ambiguity of whether a single or multiple domains should be simulated. Specifically, our unbiased first principles calculations demonstrate that a single CDW domain strongly breaks the threefold symmetry of the electronic structure, which has not been observed in experiments. Furthermore, the CDW structure shows a strong competition between nonmagnetic and magnetic states, with an energy difference of less than 5 meV/f.u. In the ferromagnetic and antiferromagnetic CDW states, the band dispersions and Fermi surface are similar to those in the nonmagnetic state. These theoretical results indicate the possibility of antiferromagnetic fluctuations in VSe_2 coexisting with the $\sqrt{3} \times \sqrt{7}$ CDW, providing a different perspective on the magnetism in monolayer VSe_2 and related CDW compounds.

II. METHODS

First-principles calculations were performed using density functional theory in the Vienna Ab-initio Simulation Package (VASP) [31,32]. The projector augmented wave pseudopotentials [33,34] were applied within the Perdew-Burke-Ernzerhof functional of the generalized gradient approximation (GGA) [35]. An energy cutoff of 320 eV is used for the plane waves [19]. The valence electrons of V and Se atoms are in the $3p^6 3d^4 4s^1$ and $4s^2 4p^4$ states, respectively. The planar lattice constant of VSe_2 monolayer is fixed to its experimental value of $a = 3.36$ Å [19,36]. The Brillouin zone is sampled with a Γ-centered $18 \times 18 \times 1$ k point mesh for the VSe_2 monolayer primitive cell. We also tested the effect of Hubbard U corrections within the V $3d$ shell in monolayer VSe_2. As shown in Fig. S1 of the Supplemental Material [37], the Hubbard U correction moves the electronic band around the Fermi level (marked red) upward and away from its nearest valence band. At $U = 0$ eV, the energy difference between the Fermi cross band and its nearest valence band at the Γ point is 0.19 eV, which is consistent with the ARPES results in previous experiments [19,22], while, this energy difference becomes 0.27 eV using $U = 1$ eV, 0.56 eV using $U = 3$ eV, and 1.00 eV with $U = 5$ eV, which is far from the experimental results. Besides, according to the ARPES results [19,22], this Fermi cross band at the Γ point is located at the Fermi level or even below the Fermi level. While, the U effect will push the red-marked band away from the Fermi level. Therefore, we did not include the Hubbard U correction in further analysis of band dispersion and Fermi surface.

The Brillouin zone was sampled with a Γ-centered $10 \times 7 \times 1$ k point mesh for the monolayer VSe_2 supercell with $\sqrt{3} \times \sqrt{7}$ periodicity, a $10 \times 3 \times 1$ k point mesh for the $\sqrt{3} \times 2\sqrt{7}$ monolayer VSe_2 supercell, and a $6 \times 4 \times 1$ k point mesh for the $2\sqrt{3} \times 2\sqrt{7}$ monolayer VSe_2 supercell. The $\sqrt{3} \times \sqrt{7}$ monolayer VSe_2 supercell is built as shown in Fig. 1(a). To mitigate interaction between periodic images, a vacuum thickness of 20 Å is used in the direction perpendicular to the monolayer. The atomic coordinates in the VSe_2 monolayer primitive cell and supercell were fully relaxed in the nonmagnetic state. The phonon dispersion of the VSe_2 primitive cell gives an imaginary mode at $3/5\Gamma K$, corresponding to a $\sqrt{3} \times \sqrt{7}$ structure instability [19,22,38]. For the initial atomic positions, we displace the V atoms by 0.12 and 0.18 Å, along the same directions as the displacement of the V atoms in the relaxed structure published in Ref. [22]. From there we fully relaxed the atomic coordinates. The relaxed $\sqrt{3} \times \sqrt{7}$ monolayer VSe_2 CDW structure is shown in Fig. 1(b). The convergence criteria for the energy and the atomic forces are 10^{-6} eV and 0.001 eV/Å, respectively.

Based on the density functional theory calculations performed in VASP, we utilize the projected Wannier function method to get the tight-binding Hamiltonian [39], which enables the calculation of the unfolded Fermi surface on a dense k point mesh with significantly reduced computational cost. The V d and Se p characters are projected in the energy window of $[-6, 4]$ eV. To preserve the symmetry of the Wannier functions, we turn off the maximal localization in WANNIER90 [40]. The band dispersions obtained from the Wannier analysis are very consistent with the bands calculated via density functional theory, as shown in Figs. S2 and S3 of the Supplemental Material [37]. Using the eigenvalues and eigenvectors of the Wannier-function based Hamiltonian, the band structure and Fermi surface of the $\sqrt{3} \times \sqrt{7}$ monolayer VSe_2 supercell were unfolded into the Brillouin zone of the primitive cell with the proper spectral weight [41]. The crystal structures of the various cells have been visualized using the VESTA 3.4.7 code [42].

III. RESULTS AND DISCUSSION

As a first step, we compute the density of states (DOS), the unfolded bands, and unfolded Fermi surface from the Wannier function based tight-binding Hamiltonian of the $\sqrt{3} \times \sqrt{7}$ monolayer VSe_2 supercell without the CDW

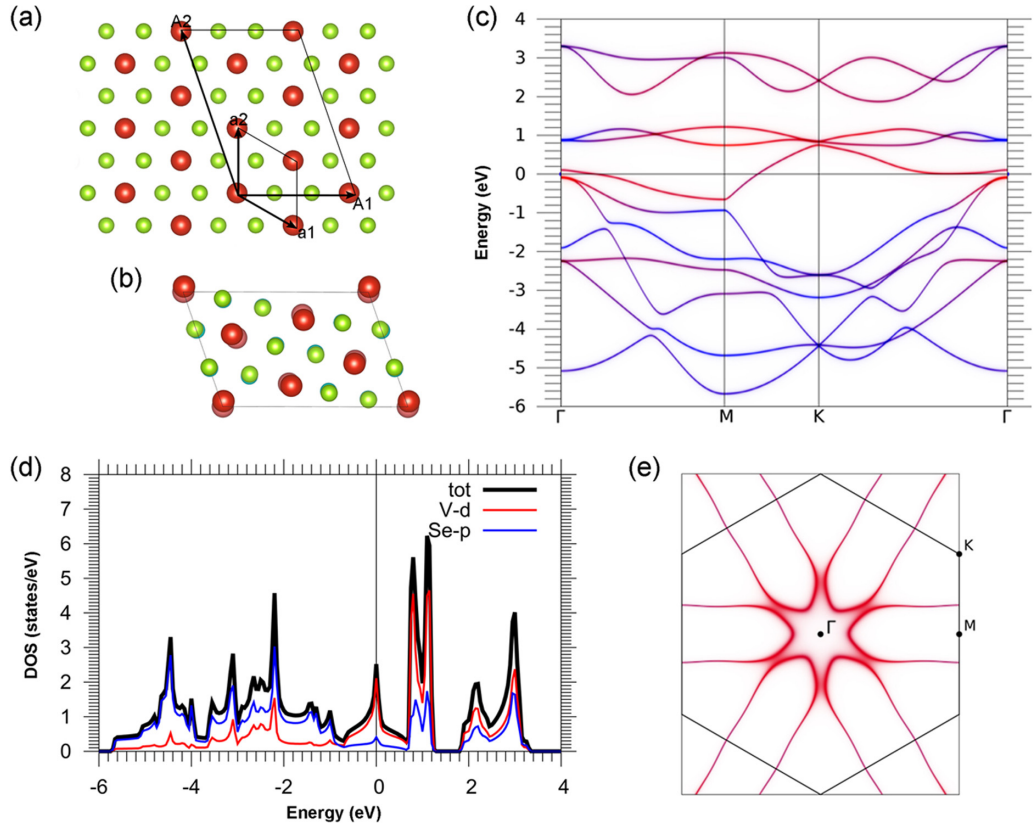

FIG. 1. (a) The geometry of the normal, i.e., undistorted, $\sqrt{3} \times \sqrt{7}$ monolayer VSe_2 supercell spanned by $A1 = 2a1 + a2$ and $A2 = -a1 + 2a2$, built from the primitive cell spanned by $a1$ and $a2$. (b) The relaxed structure of VSe_2 ($\sqrt{3} \times \sqrt{7}$) supercell with CDW. The red and green balls in (a) and (b) denote the V and Se atoms, respectively. The light red and cyan balls in (b) denotes the normal structure, i.e., the undistorted structure. The non-spin-polarized (c) unfolded band structures, (d) density of states, and (e) Fermi surface of the normal monolayer VSe_2 $\sqrt{3} \times \sqrt{7}$ supercell. The red (blue) color represents the V d (Se p) character. The Fermi level is at 0 eV.

distortions. The results are presented in Fig. 1. The Γ-centered hexagonal shape of the unfolded Fermi surface in the normal structure is consistent with the ARPES-measured Fermi surface of monolayer VSe_2 without a CDW [19], along with the M-centered ellipse-shaped electron pockets. Additionally, Fig. 1(d), shows a Van Hove singularity at the Fermi level in the undistorted nonmagnetic monolayer VSe_2. Fermi-level Van Hove singularities are well known to predispose electronic systems to various forms of energy-reducing symmetry breaking, such as the fcc-to-bct structural transition in TiH_2 [43], and have been employed as a possible explanation for high-temperature superconductivity in the cuprates [44]. Monolayer VSe_2 presents a compelling example of multiple such symmetry-breakings—magnetic order and a charge density-wave—whose exact relationship has previously eluded theoretical explanation. We intend to further examine the role of the Van Hove singularities in monolayer VSe_2 in a follow-up paper. We note that the DOS, unfolded bands, and unfolded Fermi surface from the $\sqrt{3} \times \sqrt{7}$ monolayer VSe_2 supercell without the CDW distortions (Fig. 1) are identical to those obtained from the primitive monolayer VSe_2 cell shown in Fig. S4 of the Supplemental Material [37]. While this is conceptually trivial, technically it is a good way to double check that the unfolding formalism is implemented correctly.

Next, we analyze the electronic structure of monolayer VSe_2 with the $\sqrt{3} \times \sqrt{7}$ CDW distortions. The resulting unfolded band structure is displayed in Fig. 2(a). It is found that a large CDW gap is opened in the path from M to K, which has also been observed in the experimental ARPES result [19]. We note that the 400-meV gap in our simulations is substantially

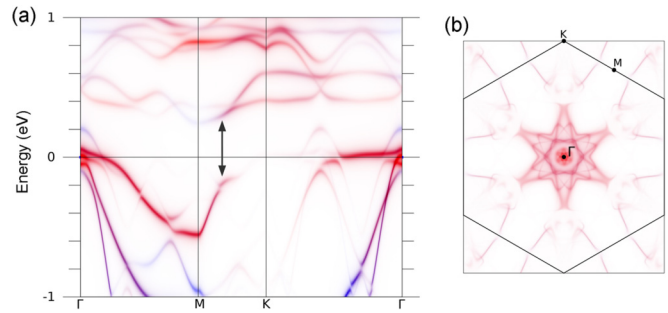

FIG. 2. The non-spin-polarized unfolded (a) band structure and (b) Fermi surface of the monolayer VSe_2 $\sqrt{3} \times \sqrt{7}$ CDW structure in the nonmagnetic state. The red (blue) color represents the V d (Se p) character. The double sided black arrow in (a) indicates the CDW gap. The Fermi level is at 0 eV. The high symmetry points in the unfolded band structure are given by $M = (0, 0.5, 0)$ and $K = (-0.333, 0.667, 0)$.

larger than the experimental CDW gap of 55 and 100 meV reported in Refs. [18] and [19] respectively. We also note that these large gap openings occur only along eight of the twelve MK paths in the hexagonal Brillouin zone. Among the other four MK paths the CDW gap opening is reduced by a factor of 10. Similarly, we note that the unfolded Fermi surface of a single $\sqrt{3} \times \sqrt{7}$ CDW domain shows a very strong breaking of the threefold symmetry that has not been observed in the ARPES experiments [see Figs. S5(b)–S5(d)]. We note that while the threefold symmetry is broken in the individual domains, it relates the unfolded bands of the three possible domains (see Fig. S5 in the Supplemental Material [37]). So, there is not one domain whose unfolded band structure is more consistent with the ARPES compared to others. Instead, we consider the possibility that the ARPES experiments to date have observed the combined spectral weight of three possible $\sqrt{3} \times \sqrt{7}$ CDW domains depicted in Fig. S5(a). Correspondingly, in this paper, we present the unfolded Fermi surfaces averaged over the three domains to facilitate the comparison with the current ARPES experiments. For the unfolded Fermi surface, the hexagram-shaped pocket around the zone center remains in the CDW structure, as shown in Fig. 2(b). However, due to the CDW gap shown in Fig. 2(a), the two long sides of the M-centered elliptical electron pockets are not as straight as those in the normal structure shown in Fig. 1(e). Such characteristics and the overall shape of the Fermi surface agree well with the previously reported ARPES [19]. However, while our unfolded Fermi surfaces agree better with the ARPES experiments when averaged over the three CDW domains, the unfolded bands do not. For two of the three CDW domains the unfolded bands display a large CDW gap opening from $M = (0, 0.5, 0)$ to $K = (-0.333, 0.667, 0)$. However, the CDW gap along this k path is strongly reduced for the third CDW domain (see Fig. S6). Therefore, when the unfolded band structures are averaged, the net result is the small CDW gap shown in Fig. S7. This leaves the question of whether the ARPES experiments on monolayer VSe_2 [19,22] have been observing the signal from all three CDW domains, or just a single one. One possible explanation of this dichotomy is that the simulations need to go beyond our approximation of averaging over the CDW domains independently. Perhaps in a more realistic approach, the bands from different domains can hybridize resulting in an intermediate CDW gap, instead of two large gaps and one small gap. This then could also explain the mismatch between the large gap size seen in the simulations compared to the ones observed in experiment. Unless there is a special symmetry, there will always be a certain degree of hybridization between the domains. If the domains are small enough then this hybridization will become significant throughout the domains, and not just at the boundaries. States that remain nongapped in an isolated domain could then open a gap. Conversely, the states that had large gaps in an isolated domain would mix with other states, which could reduce the size of the gap. We realize that this hypothesis is speculative, but what is not speculative is our unbiased first-principles result that a fixed domain strongly breaks the threefold symmetry (see Figs. S5 and S6), while no such symmetry breaking appears to be seen in ARPES. We leave such an exploration for future theoretical studies with large-sized simulations that can include multiple domains.

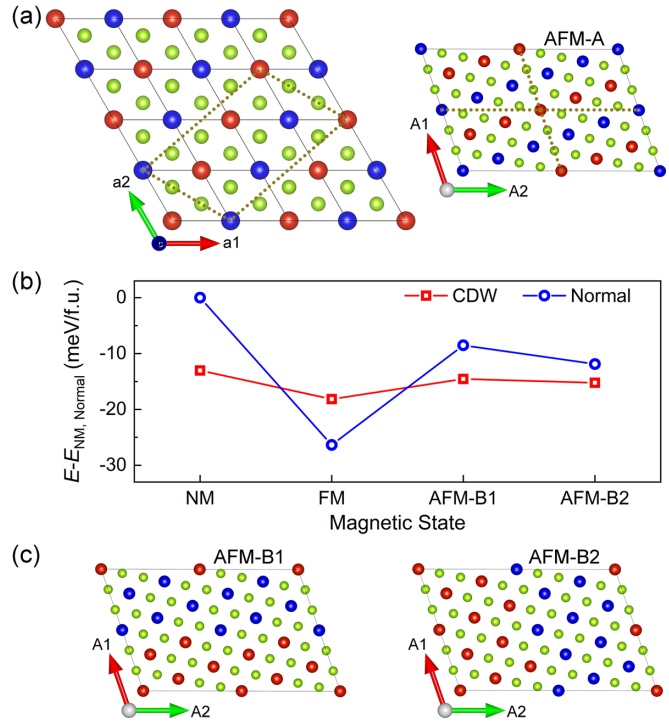

FIG. 3. (a) The frustrated antiferromagnetic order in the VSe_2 $\sqrt{3} \times \sqrt{7}$ supercell. The red and blue balls denote V atoms in the spin-up and spin-down states, respectively. (b) The energy of the VSe_2 $\sqrt{3} \times \sqrt{7}$ normal supercell and CDW structure in different magnetic states are denoted in blue and red respectively. The relevant antiferromagnetic states in (b) are displayed in (a) and (c). The energies in (b) are normalized to the energy of non-spin-polarized state in normal structure.

Also, it would be interesting if in future experiments ARPES could be performed on samples in which one CDW domain is stabilized via strain, to see if the strong symmetry breaking in the Fermi surface can be observed. Another interesting aspect of the spectral function in the CDW structure shown in Fig. 2(a) is the shadow bands within the energy interval of $[E_F - 0.25, E_F + 0.25]$ eV that are predominantly of the Se p character. This separation of the Se-p and V-d characters in monolayer VSe_2 within the CDW state may provide insight on elucidating the reported Se-distortion-affected CDW in VSe_2 [25].

Next, we explore possible magnetic states of the CDW structure, including both ferromagnetic and antiferromagnetic states. To capture the antiferromagnetic state, the $\sqrt{3} \times \sqrt{7}$ CDW supercell is further expanded to have $2\sqrt{3} \times 2\sqrt{7}$ periodicity. Considering the triangular V sublattice in VSe_2, a frustrated antiferromagnetic order is first considered. The corresponding antiferromagnetic order in the $\sqrt{3} \times \sqrt{7}$ monolayer VSe_2 supercell is displayed in Fig. 3(a), which is defined as the AFM-A order in this work. It should be noted that, in the AFM-A order, the single $\sqrt{3} \times \sqrt{7}$ supercell is ferrimagnetic. In other words, the single $\sqrt{3} \times \sqrt{7}$ supercell in the AFM-A order contains either three up spins and two down spins, or two up spins and three down spins. Additionally, we set up other antiferromagnetic orders on the basis that the single $\sqrt{3} \times \sqrt{7}$ supercell is ferromagnetic, which are defined as the AFM-B1, AFM-B2, and AFM-B3 orders

shown in Fig. 3(c). However, following the energy minimum principle, the AFM-A order in the CDW structure was found to be unstable, and relaxed to the AFM-B2 order in our simulations. Thus, we ignore the AFM-A order in further band dispersion and Fermi surface analysis, and emphasize on the AFM-B1 and AFM-B2 orders. We summarized the total energies of the CDW structure in the nonmagnetic and different magnetic states in Fig. 3(b). It is found that the energies of the CDW structure in nonmagnetic, ferromagnetic, and antiferromagnetic states are very similar to each other, with a difference of less than 5 meV/f.u. Here, f.u. denotes the formula unit, i.e., the unit cell containing one V and two Se atoms. However, in the undistorted VSe_2 $\sqrt{3} \times \sqrt{7}$ supercell, the energy difference between nonmagnetic, ferromagnetic, and antiferromagnetic states can be as high as 26 meV/f.u. We have found the spin-orbit coupling (SOC) has a minimal effect on the total energies of the $\sqrt{3} \times \sqrt{7}$ CDW structure in the nonmagnetic (NM), ferromagnetic (FM), and antiferromagnetic AFM-B2 states (see Supplemental Material Table S1 [37]). These results indicate that, as suggested previously [22], a strong competition between nonmagnetic and magnetic states exists in the CDW structure. Previous calculations showed that the U effect is important for the calculated magnetic moment of monolayer VSe_2 in the ferromagnetic state, which varies from 0.6 μ_B to 1.1 μ_B upon changing the Hubbard U from 0 to 1 eV [27]. To study the influence of Hubbard U on the proximity of AFM states, we redid the total energy analysis of various magnetic and nonmagnetic states in the CDW and normal undistorted structure (Table S2 of Supplemental Material [37]), using a Hubbard U of 1 eV. Interestingly, we found that, in this case, the AFM-A state becomes energetically the most favorable in the CDW structure, while in the normal undistorted structure, the FM state remains the lowest energy configuration. However, we also found that the corresponding unfolded Fermi surface of the AFM-A state is almost completely gapped out (see Fig. S8). Therefore, in this work we focus on the results without Hubbard U corrections.

We also compare the energy difference of monolayer VSe_2 with and without CDW. As shown in Fig. 3(b), in both the nonmagnetic and antiferromagnetic states, the CDW structure is more energetically favorable than the normal structure. On the other hand, in the ferromagnetic state the normal structure is energetically more favorable than the CDW structure. So, the ferromagnetic order is weakened as monolayer VSe_2 changes from the normal to the CDW phase, implying that the CDW suppresses ferromagnetic order as stated in previous reports [22,45]. We further unfolded the bands of the FM ordered CDW structure. As shown in Fig. 4, the exchange splitting energy can be roughly estimated to be 0.3 eV around the Γ and the M point, which is two times smaller than the exchange splitting energy in the normal structure (see Fig. S9). This reduction in the exchange splitting is consistent with our total energy calculations presented in Fig. 3(b) [37]. Just like in the nonmagnetic case, the FM case shows a CDW gap opening along the M-K panel as shown in Fig. 4. Within the individual spin channels, the spin gap is about 400 meV. However, due to the exchange splitting, the total gap will reduce to about 250 meV when the spin-up and spin-down unfolded bands are superimposed.

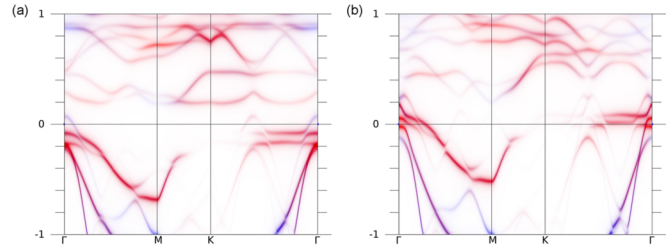

FIG. 4. The (a) spin up and (b) spin down unfolded bands in the monolayer VSe_2 $\sqrt{3} \times \sqrt{7}$ CDW structure with ferromagnetic order. The red (blue) color in the band structure represents the V d (Se p) character. The Fermi level is at 0 eV. The high symmetry points in the unfolded band structure are given by $M = (0, 0.5, 0)$ and $K = (-0.333, 0.667, 0)$.

Next, we explore the antiferromagnetic state in the monolayer VSe_2 $\sqrt{3} \times \sqrt{7}$ CDW structure. As we discussed above, the unfolded bands and Fermi surface of the monolayer VSe_2 $\sqrt{3} \times \sqrt{7}$ CDW structure in the nonmagnetic state (Fig. 2) are similar to the experimental ARPES results. Since the antiferromagnetic state is energetically favorable compared to the nonmagnetic state, we further analyze its electronic structure. Given that the AFM-B2 state has a lower energy than AFM-B1, we choose the AFM-B2 order as an example. As shown in Fig. 5(a), the band contours are very similar to the bands in the nonmagnetic state shown in Fig. 2(a). In the AFM-B2 state, especially, we again see a large CDW gap opening in the unfolded band along M to K. We further calculate the energy surface map at the Fermi level. As shown in Fig. 5(b), this map contains a large gap opening along Γ to K and a clear hexagram-shaped hole pocket around the Γ center, which is qualitatively similar to that in the nonmagnetic state shown in Fig. 2(b) and the ARPES measurements on monolayer VSe_2 in the CDW state [19]. So, in the antiferromagnetic state of AFM-B2, the energy gap from M to K exists near the Fermi level, along with the Γ-centered hexagram-shaped hole pocket. These results indicate that, in addition to the nonmagnetic state, the antiferromagnetic state has the potential to compete with the CDW structure. Our results suggest that the relationship between the CDW and magnetism in

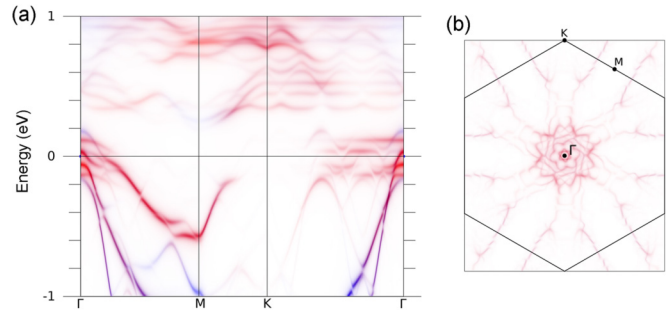

FIG. 5. The spin up/down unfolded (a) band structure and (b) Fermi surface in the monolayer VSe_2 $\sqrt{3} \times \sqrt{7}$ CDW structure with the antiferromagnetic order of AFM-B2, defined in Fig. 3(c). The red (blue) color in the band structures represents the V d (Se p) character. The Fermi level is at 0 eV. The high symmetry points in the unfolded band structure are given by $M = (0, 0.5, 0)$ and $K = (-0.333, 0.667, 0)$.

this monolayer material could be more complicated than is usually assumed. Instead of a simple competition between the CDW and the FM state, there could be a competition between the CDW state and multiple magnetic and nonmagnetic states. Further experimental probes, such as the spin-polarized scanning tunneling microscopy, may elucidate the interplay between magnetism and the CDW.

IV. CONCLUSION

Using density functional theory, Wannier function calculations, and band unfolding methods, we study the electronic structure of the monolayer VSe_2 $\sqrt{3} \times \sqrt{7}$ CDW. Certain qualitative aspects of the unfolded band dispersion and unfolded Fermi surface are similar to previous ARPES results, although there is an uncertainty about whether the ARPES probes a single domain or multiple domains. Specifically, we find that an isolated CDW domain strongly breaks the threefold symmetry of the electronic structure of monolayer VSe_2, which has not been considered in the analysis of ARPES experiments on this compound. Moreover, as compared with the normal structure, monolayer VSe_2 with the CDW structure hosts a strong competition between nonmagnetic and magnetic states, with an energy difference less than 5 meV/f.u. For the CDW structure in the ferromagnetic state, the unfolded bands display a large exchange splitting not seen in experiments. On the other hand, for the AFM CDW structure, the band dispersions and Fermi surface map are similar to those in the nonmagnetic state. The qualitative electronic characteristics and the total energies being comparable for the various magnetic and nonmagnetic states indicate the possibility that in monolayer VSe_2 the CDW order and the FM order are not only competing against each other, but also against various AFM orders.

ACKNOWLEDGMENTS

This research was supported by the U.S. Department of Energy (DOE), Office of Science, Basic Energy Sciences, Materials Sciences and Engineering Division. This research used resources of the Compute and Data Environment for Science (CADES) at the Oak Ridge National Laboratory (ORNL), which is supported by the Office of Science of the U.S. Department of Energy under Contract No. DE-AC05-00OR22725. The Department of Energy will provide public access to these results of federally sponsored research in accordance with the DOE Public Access Plan.

This manuscript has been authored by UT-Battelle, LLC under Contract No. DE-AC05-00OR22725 with the U.S. Department of Energy. The United States Government retains and the publisher, by accepting the article for publication, acknowledges that the United States Government retains a nonexclusive, paid-up, irrevocable, worldwide license to publish or reproduce the published form of this manuscript, or allow others to do so, for United States Government purposes. The Department of Energy will provide public access to these results of federally sponsored research in accordance with the DOE Public Access Plan [46].

[1] J. Dong, L. Zhang, X. Dai, and F. Ding, Nat. Commun. **11**, 5862 (2020).
[2] Z. Li, Y. Lv, L. Ren, J. Li, L. Kong, Y. Zeng, Q. Tao, R. Wu, H. Ma, B. Zhao, D. Wang, W. Dang, K. Chen, L. Liao, X. Duan, X. Duan, and Y. Liu, Nat. Commun. **11**, 1151 (2020).
[3] A. R. Oganov, C. J. Pickard, Q. Zhu, and R. J. Needs, Nat. Rev. Mater. **4**, 331 (2019).
[4] M. Gibertini, M. Koperski, A. F. Morpurgo, and K. S. Novoselov, Nat. Nanotechnol. **14**, 408 (2019).
[5] B. Huang, M. A. McGuire, A. F. May, D. Xiao, P. Jarillo-Herrero, and X. Xu, Nat. Mater. **19**, 1276 (2020).
[6] S. Kezilebieke, M. N. Huda, V. Vaňo, M. Aapro, S. C. Ganguli, O. J. Silveira, S. Głodzik, A. S. Foster, T. Ojanen, and P. Liljeroth, Nature (London) **588**, 424 (2020).
[7] K. S. Novoselov, A. Mishchenko, A. Carvalho, and A. H. Castro Neto, Science **353**, aac9439 (2016).
[8] Z. Guan, H. Hu, X. Shen, P. Xiang, N. Zhong, J. Chu, and C. Duan, Adv. Electron. Mater. **6**, 1900818 (2020).
[9] C. Gong, L. Li, Z. Li, H. Ji, A. Stern, Y. Xia, T. Cao, W. Bao, C. Wang, Y. Wang, Z. Q. Qiu, R. J. Cava, S. G. Louie, J. Xia, and X. Zhang, Nature (London) **546**, 265 (2017).
[10] B. Huang, G. Clark, E. Navarro-Moratalla, D. R. Klein, R. Cheng, K. L. Seyler, D. Zhong, E. Schmidgall, M. A. McGuire, D. H. Cobden, W. Yao, D. Xiao, P. Jarillo-Herrero, and X. Xu, Nature (London) **546**, 270 (2017).
[11] E. Ising, Z. Phys. **31**, 253 (1925).
[12] W. Lenz, Phys. Z. **21**, 613 (1920).
[13] S. T. Bramwell and P. C. W. Holdsworth, J. Phys.: Condens. Matter **5**, L53 (1993).
[14] J. M. Kosterlitz and D. J. Thouless, J. Phys. C: Solid State Phys. **6**, 1181 (1973).
[15] W. Heisenberg, Z. Phys. **49**, 619 (1928).
[16] Z. Fei, B. Huang, P. Malinowski, W. Wang, T. Song, J. Sanchez, W. Yao, D. Xiao, X. Zhu, A. F. May, W. Wu, D. H. Cobden, J.-H. Chu, and X. Xu, Nat. Mater. **17**, 778 (2018).
[17] A. F. May, S. Calder, C. Cantoni, H. Cao, and M. A. McGuire, Phys. Rev. B **93**, 014411 (2016).
[18] M. Bonilla, S. Kolekar, Y. Ma, H. C. Diaz, V. Kalappattil, R. Das, T. Eggers, H. R. Gutierrez, M.-H. Phan, and M. Batzill, Nat. Nanotechnol. **13**, 289 (2018).
[19] P. Chen, W. W. Pai, Y. H. Chan, V. Madhavan, M. Y. Chou, S. K. Mo, A. V. Fedorov, and T. C. Chiang, Phys. Rev. Lett. **121**, 196402 (2018).
[20] J. Feng, D. Biswas, A. Rajan, M. D. Watson, F. Mazzola, O. J. Clark, K. Underwood, I. Marković, M. McLaren, A. Hunter, D. M. Burn, L. B. Duffy, S. Barua, G. Balakrishnan, F. Bertran, P. Le Fèvre, T. K. Kim, G. van der Laan, T. Hesjedal, P. Wahl, and P. D. C. King, Nano Lett. **18**, 4493 (2018).
[21] W. Zhang, L. Zhang, P. K. J. Wong, J. Yuan, G. Vinai, P. Torelli, G. van der Laan, Y. P. Feng, and A. T. S. Wee, ACS Nano **13**, 8997 (2019).
[22] P. M. Coelho, K. Nguyen Cong, M. Bonilla, S. Kolekar, M.-H. Phan, J. Avila, M. C. Asensio, I. I. Oleynik, and M. Batzill, J. Phys. Chem. C **123**, 14089 (2019).

[23] M. Hossain, Z. Zhao, W. Wen, X. Wang, J. Wu, and L. Xie, Crystallography **7**, 298 (2017).
[24] G. Duvjir, B. K. Choi, I. Jang, S. Ulstrup, S. Kang, T. Thi Ly, S. Kim, Y. H. Choi, C. Jozwiak, A. Bostwick, E. Rotenberg, J.-G. Park, R. Sankar, K.-S. Kim, J. Kim, and Y. J. Chang, Nano Lett. **18**, 5432 (2018).
[25] T. T. Ly, G. Duvjir, N. H. Lam, J. Kim, B. K. Choi, and Y. J. Chang, J. Korean Phys. Soc. **76**, 412 (2020).
[26] P. K. J. Wong, W. Zhang, F. Bussolotti, X. Yin, T. S. Herng, L. Zhang, Y. L. Huang, G. Vinai, S. Krishnamurthi, D. W. Bukhvalov, Y. J. Zheng, R. Chua, A. T. N'Diaye, S. A. Morton, C.-Y. Yang, K.-H. Ou Yang, P. Torelli, W. Chen, K. E. J. Goh, J. Ding *et al.*, Adv. Mater. **31**, 1901185 (2019).
[27] M. Esters, R. G. Hennig, and D. C. Johnson, Phys. Rev. B **96**, 235147 (2017).
[28] Y. Ma, Y. Dai, M. Guo, C. Niu, Y. Zhu, and B. Huang, ACS Nano **6**, 1695 (2012).
[29] W. Yu, J. Li, T. S. Herng, Z. Wang, X. Zhao, X. Chi, W. Fu, I. Abdelwahab, J. Zhou, J. Dan, Z. Chen, Z. Chen, Z. Li, J. Lu, S. J. Pennycook, Y. P. Feng, J. Ding, and K. P. Loh, Adv. Mater. **31**, 1903779 (2019).
[30] R. Chua, J. Yang, X. He, X. Yu, W. Yu, F. Bussolotti, P. K. J. Wong, K. P. Loh, M. B. H. Breese, K. E. J. Goh, Y. L. Huang, and A. T. S. Wee, Adv. Mater. **32**, 2000693 (2020).
[31] G. Kresse and J. Furthmüller, Comput. Mater. Sci. **6**, 15 (1996).
[32] G. Kresse and J. Furthmüller, Phys. Rev. B **54**, 11169 (1996).
[33] P. E. Blöchl, Phys. Rev. B **50**, 17953 (1994).
[34] G. Kresse and D. Joubert, Phys. Rev. B **59**, 1758 (1999).
[35] J. P. Perdew, K. Burke, and M. Ernzerhof, Phys. Rev. Lett. **77**, 3865 (1996).
[36] G. A. Wiegers, Physica B+C **99**, 151 (1980).
[37] See Supplemental Material at http://link.aps.org/supplemental/10.1103/PhysRevB.106.085117 for more details about the electronic structure of monolayer VSe_2 in normal and CDW structures.
[38] J. G. Si, W. J. Lu, H. Y. Wu, H. Y. Lv, X. Liang, Q. J. Li, and Y. P. Sun, Phys. Rev. B **101**, 235405 (2020).
[39] W. Ku, H. Rosner, W. E. Pickett, and R. T. Scalettar, Phys. Rev. Lett. **89**, 167204 (2002).
[40] A. A. Mostofi, J. R. Yates, Y.-S. Lee, I. Souza, D. Vanderbilt, and N. Marzari, Comput. Phys. Commun. **178**, 685 (2008).
[41] W. Ku, T. Berlijn, and C.-C. Lee, Phys. Rev. Lett. **104**, 216401 (2010).
[42] K. Momma and F. Izumi, J. Appl. Crystallogr. **44**, 1272 (2011).
[43] K. V. Shanavas, L. Lindsay, and D. S. Parker, Sci. Rep. **6**, 28102 (2016).
[44] E. Dagotto, A. Nazarenko, and A. Moreo, Phys. Rev. Lett. **74**, 310 (1995).
[45] T. J. Kim, S. Ryee, M. J. Han, and S. Choi, 2D Mater. **7**, 035023 (2020).
[46] http://energy.gov/downloads/doe-public-access-plan.